Identifying neuronal oscillations using rhythmicity

Fransen, A.M.M.; Ede, F.L. van; Maris, E.G.G.

2015, Article / Letter to editor (NeuroImage, 118, (2015), pp. 256-267)

Doi link to publisher: https://doi.org/10.1016/j.neuroimage.2015.06.003

NeuroImage 118 (2015) 256–267

Contents lists available at ScienceDirect

NeuroImage

journal homepage: www.elsevier.com/locate/ynimg

Identifying neuronal oscillations using rhythmicity

Anne M.M. Fransen, Freek van Ede, Eric Maris *

Radboud University, Donders Institute for Brain, Cognition and Behaviour, Nijmegen, The Netherlands

ARTICLE INFO

Article history:
Received 12 January 2015
Accepted 1 June 2015
Available online 6 June 2015

Keywords:
Rhythmicity
Neuronal oscillations
Phase preservation
Lagged coherence
Spatial attention
Sensorimotor rhythms

ABSTRACT

Neuronal oscillations are a characteristic feature of neuronal activity and are typically investigated through measures of power and coherence. However, neither of these measures directly reflects the distinctive feature of oscillations: their rhythmicity. Rhythmicity is the extent to which future phases can be predicted from the present one. Here, we present *lagged coherence*, a frequency-indexed measure that quantifies the rhythmicity of neuronal activity. We use this method to identify the sensorimotor alpha and beta rhythms in ongoing magnetoencephalographic (MEG) data, and to study their attentional modulation. Using lagged coherence, the sensorimotor rhythms become visible in ongoing activity as local rhythmicity peaks that are separated from the strong posterior activity in the same frequency bands. In contrast, using conventional power analyses, the sensorimotor rhythms cannot be identified in ongoing data, nor can they be separated from the posterior activity. We go on to show that the attentional modulation of these rhythms is also evident in lagged coherence and moreover, that in contrast to power, it can be visualised even without an experimental contrast. These findings suggest that the rhythmicity of neuronal activity is better suited to identify neuronal oscillations than the power in the same frequency band.

Introduction

Neuronal oscillations are a fundamental aspect of brain signalling (Buzsáki and Draguhn, 2004); this holds for the whole range from sensory processing (Koepsell et al., 2010) to motor control (Engel and Fries, 2010; Davis et al., 2012), including neuronal communication (Fries, 2005), computation (Fries, 2009), and cognitive function (Ward, 2003; Düzel et al., 2010; Bosman et al., 2014). The distinctive feature of neuronal oscillations is its repetitive nature: a periodic waveform allows for the prediction of future phases on the basis of the present one. We denote this feature by the term *rhythmicity*: the more periodic the waveform, the more rhythmic the signal, and the better future phases can be predicted. In the most extreme case of a perfectly rhythmic signal, phase is a perfectly linear function of time.

Neuronal activity is not entirely oscillatory, but also comprises transient activity. Because rhythmic and transient signals most likely originate from different neuronal mechanisms (Kaneoke and Vitek, 1996; Riehle et al., 1997; Chan et al., 2011; Fetz, 2013), it is important to differentiate between them. Methodological efforts to resolve this ambiguity between transient and rhythmic activity were most successful in the analyses of spike trains (Kaneoke and Vitek, 1996). Kaneoke and Vitek (1996) describe separate analyses methods to identify bursts (high amplitude transients) and rhythmic discharges (oscillations). Unfortunately these methods do not translate well to field potentials. In field potentials, efforts to differentiate rhythms from transients have thus far concentrated on signal decomposition methods such as matching pursuit (Wacker and Witte, 2013; Gross, 2014). Matching pursuit decomposes a signal as a sum of so-called *atoms* from a predefined dictionary (Mallat and Zhang, 1993). Provided this dictionary contains both oscillatory and non-oscillatory atoms (with the oscillatory ones extending over several cycles), the rhythmicity of a signal is reflected indirectly by the duration of the selected atoms (i.e., their number of cycles).

In contrast to these studies, neuronal oscillations are typically investigated using tools based on or inspired by the Fourier transform (Wacker and Witte, 2013; Gross, 2014). The Fourier transform dissects a signal into a set of sinusoidal components, such that the sum of all components perfectly describes the observed signal. From this transform, a *Fourier power* spectrum is typically calculated, and peaks in this spectrum are interpreted as identifiers of neuronal oscillations. This is a sloppy interpretation because it ignores the fact that Fourier power not only reflects the average amplitude of sinusoids, but also of transient activity. This is especially troubling, because neuronal activity exhibits irregular high-amplitude transients (Freyer et al., 2009). Some peaks in the Fourier power spectrum may reflect such irregular high-amplitude transients rather than oscillations.

To illustrate this, we dissociate rhythmicity and power in three 0.6 s long example signals, shown in Fig. 1A. At this point, it is useful to have a definition of rhythmicity from which a measure can be derived. In our definition rhythmicity is a frequency-indexed measure, and it assumes a particular time window length over which a signal's phase

* Corresponding author at: Radboud University, Donders Institute for Brain, Cognition and Behaviour, Nijmegen, The Netherlands, Montessorilaan 3, 6525 HR Nijmegen, P.O. Box 9104, 6500 HE Nijmegen, The Netherlands. Fax: +31 243616066.
E-mail address: e.maris@donders.ru.nl (E. Maris).

http://dx.doi.org/10.1016/j.neuroimage.2015.06.003
1053-8119/

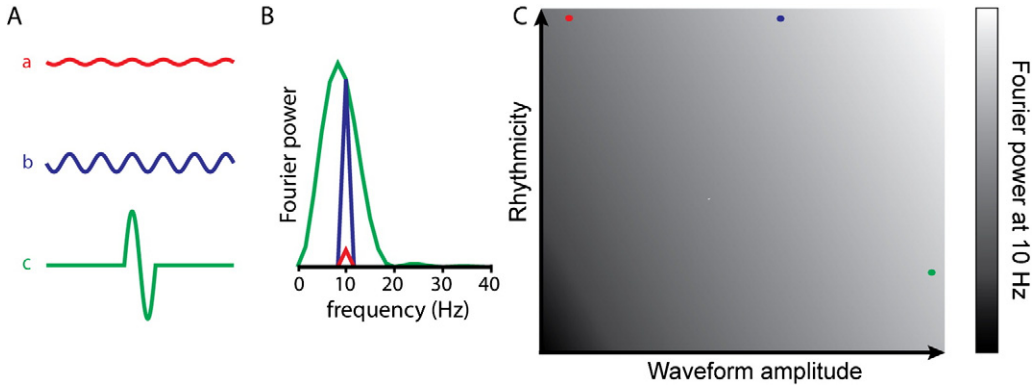

Fig. 1. Fourier power depends on both waveform amplitude and waveform rhythmicity. (A) Waveforms can vary in their average amplitude and rhythmicity. Waveforms *a* and *b* have the same rhythmicity and only differ in their waveform amplitude, whereas waveforms *b* and *c* have the same Fourier power at 10 Hz, but differ in both their rhythmicity and waveform amplitude. (B) Fourier power spectra for signals *a*, *b*, and *c*. (C) Each coloured dot describes the identically coloured waveform in A by its waveform amplitude (plotted on the horizontal axis) and its rhythmicity (plotted on the vertical axis). The Fourier power at 10 Hz is plotted as a function of both waveform amplitude and rhythmicity. Many combinations of waveform amplitude and rhythmicity result in the same Fourier power (i.e. all locations with the same shade of grey). For example, it is possible that signals with less rhythmicity, have a higher Fourier power (such as signal *c* (green) versus signal *a* (red)). The image in panel C is a schematic only; its geometrical relations do not pretend to reflect relations that can be deduced by a formal proof.

is estimated. Let this window length be denoted by *T*. Then, rhythmicity at some frequency is the consistency between these frequency-specific phases across adjacent non-overlapping time windows of length *T*. If a signal is perfectly rhythmic (such as sinusoids), future phases can be fully predicted and the rhythmicity of the signal is 1. On the other hand, if the signal is fully arrhythmic (such as white noise) the future phases are fully unpredictable, and the rhythmicity is 0. To return to Fourier power spectra of transients compared to sinusoids, all signals in Fig. 1A are based on a 0.1 s long sinusoidal waveform, and we are interested in the Fourier power for the corresponding frequency (10 Hz). The first two signals (*a*, *b*) are perfectly rhythmic: the waveform repeats itself periodically, resulting in a phase that is a perfectly linear function of time. The third signal (*c*) is not rhythmic and is typically denoted as a transient. In the example signals with identical rhythmicity (Fig. 1, *a*, *b*), the Fourier power only reflects waveform amplitude (Fig. 1B). The Fourier power spectrum of signal *c* also contains a peak in the alpha band (7–15 Hz), and at 10 Hz its Fourier power is equal to that of signal *b*. This means that when both rhythmicity and waveform amplitude are allowed to vary, the Fourier power at a given frequency can reflect a whole range of phenomena, from a low-amplitude oscillation to a high-amplitude transient (namely all locations in Fig. 1C with identical shade of grey).

To understand this, it is important to know that the mean square of signal *c* is larger than that of signal *b* (with the mean square in this case being proportional to the number of waveforms times the squared waveform amplitude). Parseval's theorem states that the Fourier transform separates a signal's mean square into Fourier power values across the different frequencies. One of these frequencies is the frequency of interest (in this case 10 Hz). The more rhythmic a signal, the more its energy is concentrated in this frequency of interest (Fig. 1B, compare the blue and green curves). This explains why, compared to a transient signal, a rhythmic signal requires a smaller waveform amplitude in order to have the same Fourier power at this frequency of interest. Thus, Fourier power at a given frequency reflects both the rhythmicity and the waveform amplitude at that frequency, without discriminating between them.

In this paper, we present a direct measure of rhythmicity, and show that it can be used to detect neuronal oscillations as well as their modulations by task demands. This measure is called *lagged coherence* and its calculation is analogous to the familiar coherence measure that is used to quantify the consistency of the phase relations between two recording sites. Rather than quantifying phase consistency between recording sites, lagged coherence quantifies phase consistency between different time intervals at the same recording site. Disregarding effects of noise (see Discussion) lagged coherence does not depend on waveform amplitude and, contrary to Fourier power, it differentiates between rhythmic signals and transients.

First, we introduce lagged coherence and its dependence on lag. Next, we demonstrate its usefulness in the analysis of MEG data, and compare these results with those obtained using conventional Fourier power. Specifically, we demonstrate the unique ability of lagged coherence to identify the sensorimotor alpha and beta rhythms on the basis of their spatial distribution, effectively separating these sources from the much stronger posterior sources in the same frequency bands. Finally, we show that lagged coherence can identify top-down modulations by attention within a *single* attention condition, thus without requiring the more usual contrast between conditions.

Materials and methods

Participants

We re-analysed data from two experiments (see the "Experimental design and data selection section"). In Experiment I, we obtained data from one healthy adult (male; 28 years), and in Experiment II we obtained data from eleven healthy adults (5 male; 22–49 years). All data was collected in accordance with guidelines of the Declaration of Helsinki and approved by the local ethics committee (CMO Regio Arnhem-Nijmegen). Informed written consent was obtained from all subjects.

Data acquisition

Neurophysiological data was collected with an MEG system (CTF MEG; MISL, Coquitlam, British Columbia, Canada) with 275 axial gradiometers, which was housed in a magnetically shielded room. The data was combined offline with T1-weighted MR images, as described in the "Source reconstruction of lagged coherence" section.

Experimental design and data selection

We used single subject data of Experiment 1 to demonstrate the dependence of lagged coherence on lag (Fig. 3). This MEG dataset contains long epochs without experimental events. More specifically, it consists of 8 s epochs in which subjects were instructed in alternation to keep their eyes open or closed. Approximately 1500 trials were collected. Because this dataset served a demonstrative purpose only, we confined our analysis to the eyes-closed trials of the first participant.

The data acquisition and experimental design for experiment II are described in full detail in van Ede et al. (2012). In short, the experiment consists of a cued sensorimotor detection task, in which the task was to report the presence or absence of a weak electro-tactile stimulus on the left or right thumb. A stimulus was presented in 50% of the trials. In 33% of the trials, the location (left/right) at which the stimulus could occur was cued 1.5 s prior to stimulation using a 0.15 s auditory cue. In the remaining trials, no preparatory cue was provided. The data epochs of interest were the last second before the onset of the electro-tactile stimulus in stimulus-present trials or the equivalent epoch in stimulus-absent trials. This resulted in approximately 1200 trials per subject, 800 of which were uncued. For this dataset, we collected T1-weighted MR images, and thus were able to perform source reconstructions.

Data pre-processing

Data were analysed using FieldTrip (Oostenveld et al., 2011), an open-source MATLAB toolbox developed at the Donders Institute for Brain, Cognition and Behaviour (Nijmegen, The Netherlands) together with custom-written code. We removed line noise by means of the discrete Fourier transform (DFT) and we removed the direct current component of each epoch by subtracting its mean. All epochs of interest were visually inspected for the presence of artefacts in a semi-automated fashion using variance, kurtosis and the maximum absolute value in each recording site. Contaminated epochs were removed from the data.

Calculating power spectra

Power spectra were calculated using multitaper estimation (Percival and Walden, 1993). We used a frequency smoothing of 4 Hz on either side of the centre frequency. This frequency smoothing comes close to the smoothing produced by the three-cycle Hanning-tapered windowed Fourier transform on which we based our calculation of lagged coherence. Multitaper estimation was only used for the power spectra; the Fourier power values that were used for calculating lagged coherence were all based on a three-cycle Hanning-tapered windowed Fourier transform.

Calculating lagged coherence

Lagged coherence measures rhythmicity, which we define as the consistency of the phase relations between time points that are separated by some interval (lag). A well-known and commonly used measure to quantify the consistency of phase relations is coherence (Rosenberg et al., 1989; Lachaux et al., 1999). Typically, this measure is used to quantify the consistency of the phase relations between simultaneous signals at different recording sites. Here, we applied this measure to signals in non-overlapping epochs recorded at the same site. The idea of calculating coherence with a time delay is not new: it was proposed by (Govindan et al., 2006) in a between-site version as a tool to investigate functional connectivity between brain sites (see, Muthuraman et al., 2008, for an application). Accordingly, lagged coherence (λ) is the coherence between a signal ($\boldsymbol{x}_n$) and the lagged version of that same signal ($\boldsymbol{x}_{n+1}$):

$$\lambda(k) = \left| \frac{\sum_{n=1}^{N-1} \mathcal{F}(\boldsymbol{x}_n)_k \mathcal{F}(\boldsymbol{x}_{n+1})_k^H}{\sqrt{\left(\sum_{n=1}^{N-1} |\mathcal{F}(\boldsymbol{x}_n)_k|^2\right)\left(\sum_{n=1}^{N-1} |\mathcal{F}(\boldsymbol{x}_{n+1})_k|^2\right)}} \right| \quad (1)$$

The lagged coherence $\lambda(k)$ is a function of frequency, which we denote by its index k in the series of Fourier frequencies. In this equation, $\mathcal{F}(\boldsymbol{x}_n)$ denotes the Fourier transform of the signal $\boldsymbol{x}_n$. We follow the notational convention that all vectors (and therefore also all univariate signals) are denoted as lowercase bold symbols. The Fourier transform $\mathcal{F}(\boldsymbol{x}_n)$ is a vector-valued function, and we use the subscript k to select the k^{th} Fourier coefficient. Here and in the following, we will use the superscript H to denote the Hermitian (complex conjugate) transpose. When applied to a scalar, the Hermitian transpose reduces to an ordinary complex conjugate. We use || to denote the absolute value. The signals $\boldsymbol{x}_n$ (for n = 1,…,N) are actually ordered equal-length epochs that were cut from the original, longer, signal. In most of the applications in this paper, the epochs are adjacent and non-overlapping, although this is not necessary for the calculation of lagged coherence. To fully specify lagged coherence, we must know the epochs' lengths and their between-epoch delays. In this paper, all Fourier coefficients needed for the calculation of lagged coherence were obtained from epochs with a length of three cycles of the frequency of interest. Fourier coefficients were calculated in combination with a Hanning taper. Calculating Fourier coefficients on tapered signals with a frequency-dependent length is equivalent to the so-called wavelet method (Bruns, 2004) and the resulting coefficients are also called wavelet coefficients. In all but one analysis, the second epoch was chosen to lag behind the first one by three cycles. Thus, the second epoch directly followed the first one, without any overlap. The single exception is the analysis of which the results are shown in Fig. 3. In the analysis, the lag was varied from 3 to 20 cycles of the frequency of interest. Because in this paper these parameters are always known from the context, they will not be included in the notation.

The calculation of lagged coherence is illustrated in Fig. 2, using the signal recorded from a posterior MEG recording site, which exhibits rhythmic activity in the alpha band. We selected five adjacent epochs, with each epoch being 3 cycles long at 10 Hz (i.e. 300 ms; Fig. 2A). In the first step, we calculate the Fourier coefficient for each epoch, by Fourier transforming the Hanning-tapered signal (or, equivalently, by multiplying the signal with a 3-cycle wavelet at 10 Hz). The amplitudes and phases of these Fourier coefficients are represented by, respectively, the lengths and the angles of the vectors in Fig. 2B. In the second step, we consider each adjacent pair of epochs, and calculate the product $\mathcal{F}(\boldsymbol{x}_n)_k \mathcal{F}(\boldsymbol{x}_{n+1})_k^H$. The phase of this product equals the phase relation between the two epochs in that pair. The complex numbers $\mathcal{F}(\boldsymbol{x}_n)_k \mathcal{F}(\boldsymbol{x}_{n+1})_k^H$ are depicted in Fig. 2C, with length representing amplitude, and angle representing the phase relation between the two epochs. In the third step, we sum these complex numbers over all epoch pairs and use this as the numerator of Eq. (1). The corresponding average (the sum divided by $N-1$, the number of epoch pairs) is called the *lagged autospectrum*, and is depicted by the bold line in Fig. 2D. The amplitude of the lagged autospectrum increases with the consistency over epochs in the phase relations between the two epochs in a pair.

The denominator of Eq. (1) serves to normalise the lagged autospectrum. In fact, the lagged autospectrum does not only depend on the phases of the Fourier coefficients $\mathcal{F}(\boldsymbol{x}_n)_k$ and $\mathcal{F}(\boldsymbol{x}_{n+1})_k$, but also on their amplitudes. To correct for this dependence on amplitude, we divide the lagged autospectrum by the square-root of the power of the first and the second epoch in the set of all epoch pairs. Equivalently, we divide the numerator of Eq. (1) by the square-root of two sums of squared amplitudes: the sum of the squared amplitudes of the first and the second epoch. This results in a complex number with an absolute value between 0 and 1; this absolute value is lagged coherence.

Calculating planar gradient lagged coherence

We calculated power and lagged coherence for synthetic planar MEG gradiometers. Planar gradiometers have the advantage over axial gradiometers that, after combining the power in the two planar directions, it is maximal above the neuronal sources (Bastiaansen and Knosche, 2000). This allows for an easier interpretation of topographic maps, especially after averaging over subjects with different dipole orientations. Bastiaansen and Knosche (2000) described how to calculate planar gradiometer power from axial gradiometer signals. For lagged coherence, we performed a similar calculation.

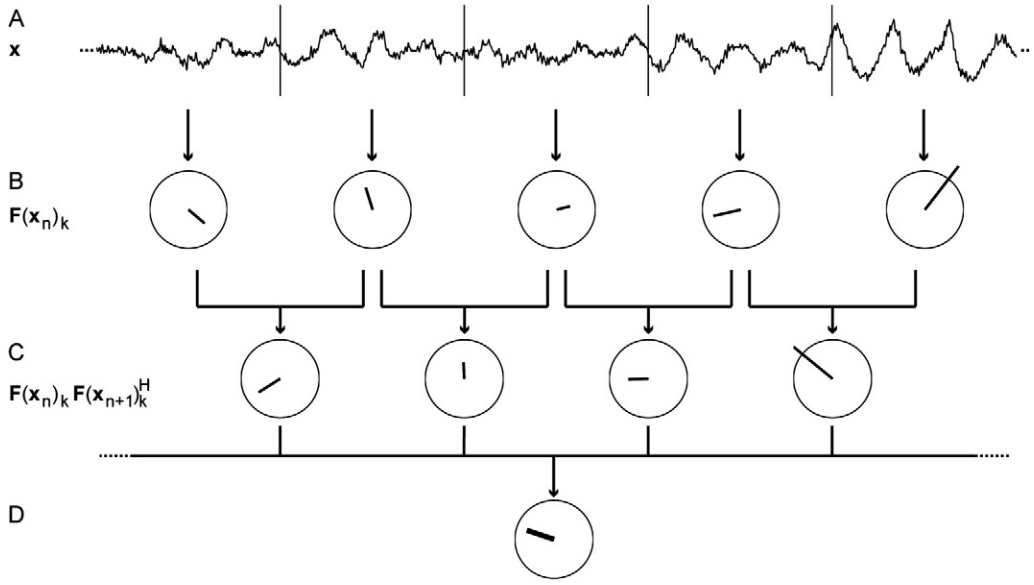

Fig. 2. Lagged coherence measures the phase consistency between non-overlapping data fragments. (A) Raw data is cut into epochs of 3 cycles of the frequency of interest. Here, 5 adjacent epochs are shown. In each pair of epochs, the first epoch (left of the vertical bar) is referred to as $\boldsymbol{x}_n$ and the second (right of the vertical bar) as $\boldsymbol{x}_{n+1}$. (B) For each epoch, the Fourier coefficient $\mathcal{F}(\boldsymbol{x}_n)_k$ is calculated, in which k is the index of the frequency of interest in the series of Fourier frequencies. Each Fourier coefficient is represented by a vector in the complex plane; the Fourier coefficient's amplitude corresponds to the vector's length, and its phase to the vector's angle relative to the positive horizontal axis. (C) The phase of the product $\mathcal{F}(\boldsymbol{x}_n)_k\mathcal{F}(\boldsymbol{x}_{n+1})_k^H$ equals the difference between the phases of $\mathcal{F}(\boldsymbol{x}_n)_k$ and $\mathcal{F}(\boldsymbol{x}_{n+1})_k$. (D) The across-epoch consistency of the phase differences in C indexes rhythmicity: the more rhythmic the signal, the more consistent the phase differences. This phase consistency can be measured by the average over the epoch pairs of the products $\mathcal{F}(\boldsymbol{x}_n)_k\mathcal{F}(\boldsymbol{x}_{n+1})_k^H$ in C. This average is the lagged autospectrum and is displayed in D. Note that the vectors in C and D are on the same scale. The amplitude of the lagged autospectrum denotes both the strength of the rhythmicity and the amplitude of the rhythm. The pure phase consistency across epochs is best measured by lagged coherence, which is calculated by normalising the lagged autospectrum by the average amplitude in all epochs used (see Eq. 1). This results in a value between 0 and 1, which quantifies the signal's rhythmicity (i.e. phase consistency across time).

To calculate planar gradient lagged coherence, we start from the first spatial derivatives of the MEG signal at the location of the sensor in the plane tangential to the MEG helmet. We calculate the spatial derivatives in the horizontal and the vertical direction of this tangential plane relative to the coordinate system of the MEG helmet, although any other pair of directions would also do (see Bastiaansen and Knosche (2000) for the details of this calculation). Next, we calculate Fourier coefficients from these signals, and denote these by, respectively, $\mathcal{F}(\boldsymbol{h}_n)_k$ and $\mathcal{F}(\boldsymbol{v}_n)_k$, in which $\boldsymbol{h}_n$ and $\boldsymbol{v}_n$denote the first spatial derivatives in the horizontal and the vertical directions.

For every site, we then combine the Fourier coefficients for the horizontal and the vertical direction into a single coefficient, namely the one for which the power is strongest. This direction of maximum power can be found by performing singular value decomposition on the real part of the 2-by-2 cross-spectral density (CSD) matrix that is obtained by averaging the outer product of the vector $\begin{bmatrix}\mathcal{F}(\boldsymbol{h}_n)_k\\ \mathcal{F}(\boldsymbol{v}_n)_k\end{bmatrix}$ with its conjugate transpose:

$$S^{planar} = 1/N\sum_{n=1}^{N}\left(\begin{bmatrix}\mathcal{F}(\boldsymbol{h}_n)_k\\ \mathcal{F}(\boldsymbol{v}_n)_k\end{bmatrix}\begin{bmatrix}\mathcal{F}(\boldsymbol{h}_n)_k^H & \mathcal{F}(\boldsymbol{v}_n)_k^H\end{bmatrix}\right)$$

Here and in the following, matrices will be denoted by capital letters. We take the real part of the CSD matrix S^{planar} because we want to find the direction of maximum power without inducing a phase shift, as is dictated by the fact that the relation between the magnetic field and its spatial derivatives is instantaneous. The singular value decomposition of $Real(S^{planar})$ can be written as follows:

$$Real\left(S^{planar}\right) = U\Sigma V^H$$

where $U = V$, because $Real(S^{planar})$ is symmetric. U is the spatial filter that holds two orthogonal directions, of which the first one (the first column of U, denoted by $\boldsymbol{u}_1$) holds the direction of the strongest power. We apply this filter to the axial gradiometer signal to obtain the planar gradient signal:

$$\boldsymbol{x}_n^{planar} = \boldsymbol{u}_n^H\begin{bmatrix}\boldsymbol{h}_n\\ \boldsymbol{v}_n\end{bmatrix}$$

where the Hermitian transpose is equivalent to the regular transpose because $\boldsymbol{u}_1$ is real-valued. In the same way, we calculate $\boldsymbol{x}_{n+1}^{planar}$ from $\boldsymbol{h}_{n+1}$ and $\boldsymbol{v}_{n+1}$. In the final step, we replace the axial gradiometer signals $\boldsymbol{x}_n$ and $\boldsymbol{x}_{n+1}$in Eq. (1) with the planar gradient signals $\boldsymbol{x}_n^{planar}$ and $\boldsymbol{x}_{n+1}^{planar}$ to obtain the planar gradient lagged coherence.

Source reconstruction of lagged coherence

Beamforming (Van Veen et al., 1997; Gross et al., 2001; Liljestrom et al., 2005) is a form of spatial filtering that is commonly used for the source reconstruction of neuronal activity. In essence, for each of the source locations of interest, the beamformer spatial filters are calculated on the basis of the sources' leadfields and the CSD matrix for the recording sites involved. These source locations of interest were obtained by discretising each individual's magnetic resonance image into a 3 dimensional grid with 1.5 cm resolution. Source lagged coherence can be reconstructed in the same way as source power, namely by using a spatial filter to calculate a synthetic signal and applying the formula for lagged coherence (Eq. 1) to this synthetic signal. However, to calculate lagged coherence, it turns out not to be necessary to also calculate this very large number of synthetic signals (one for every source location of interest). Instead, a very efficient calculation can be used, based on the so-called *lagged CSD matrix*, which will be introduced in the following. We next describe how to reconstruct the power at the source level and how this calculation is adapted for lagged coherence.

To reconstruct source power, we need the CSD matrix S_k that can be calculated from the Fourier coefficients of the multichannel signals obtained from all recording sites jointly. The spatiotemporal (channels-by-timepoints) matrix of multichannel signals of the nth epoch is

denoted by X_n, and its corresponding vector of Fourier coefficients for the k^{th} Fourier frequency by $\mathcal{F}(X_n)_k$. The CSD matrix S_k can now be calculated as follows:

To reconstruct source lagged coherence, we need a related quantity, the lagged CSD matrix LS_k, which is calculated as follows:

$$LS_k = \frac{1}{N-1}\sum_{n=1}^{N-1}\mathcal{F}(X_n)_k\mathcal{F}(X_{n+1})_k^H$$

with $\mathcal{F}(X_{n+1})_k$ the vector of Fourier coefficients of the lagged signal X_{n+1}.

Source-reconstructed power and lagged coherence can be obtained by calculating the power and lagged coherence, respectively, of a synthetic signal that is obtained by applying a spatial filter W_{ki} to the original signal X_n, with i indexing the source location of interest. This spatial filter is calculated from the CSD matrix S_k and the leadfield for the source location of interest ((Van Veen et al., 1997). Motivated by the fact that the temporal relation between the source- and the sensor-level signals is quasi-instantaneous, we do not want the spatial filter to induce a phase shift, and therefore we constrain it be real-valued. For each source location,W_{ki} is a three-column real-valued matrix, with one column for each of the three directions of the coordinate system. The application of this filter results in a 3-dimensional synthetic signal with the following 3-by-3 cross-spectral and lagged CSD matrix:

$$S_{ki}^{source} = W_{ki}^H S_k W_{ki}$$
$$LS_{ki}^{source} = W_{ki}^H LS_k W_{ki}.$$

Because we are not interested in the power and lagged coherence in all directions of our coordinate system, we only consider the directions in which these quantities are maximal. These directions are found by applying singular value decomposition to these 3-by-3 matrices. To calculate source-reconstructed lagged coherence, we apply this singular value decomposition to LS_{ki}^{source}:

$$LS_{ki}^{source} = U\Sigma V^H$$

The first singular value is the lagged autospectrum for the direction in which it is strongest. This singular value can be calculated as $\boldsymbol{u}_1^H LS_{ki}^{source}\boldsymbol{v}_1$, in which $\boldsymbol{u}_1$ and $\boldsymbol{v}_1$ are the first singular vectors that appear as the first column of U and V, respectively. This quantity corresponds to the numerator of Eq. (1), and will be called the source-reconstructed lagged autospectrum.

The last step in the calculation of the source-reconstructed lagged coherence is the normalisation of the source-reconstructed lagged autospectrum. For that, we divide the source-reconstructed lagged autospectrum by the product of two root-mean-square amplitudes: the root-mean-squares of the amplitudes that correspond to the first and the second epoch in every pair. In fact, from the calculation of LS_k, it can be seen that the rows of LS_k correspond to the signals that are denoted by X_n, which range from X_1 to X_{N-1}, and its columns correspond to the signals that are denoted by X_{n+1}, which range from X_2 to X_N. This allows us to apply the filters $\boldsymbol{u}_1$ and $\boldsymbol{v}_1$ to obtain the source power in the same direction as LS_{ki}^{source} for the signal and the lagged signal, respectively. The CSD matrices for these two sets of signals are calculated as follows:

$$S_{k1} = \frac{1}{N-1}\sum_{n=1}^{N-1}\mathcal{F}(X_n)_k\mathcal{F}(X_n)_k^H$$
$$S_{k2} = \frac{1}{N-1}\sum_{n=2}^{N}\mathcal{F}(X_n)_k\mathcal{F}(X_n)_k^H.$$

The normalisation of the source-reconstructed lagged autospectrum then produces the source-reconstructed lagged coherence:

$$\lambda^{source}(k,i) = \left|\frac{\boldsymbol{u}_1^H W_{ki}^H LS_k W_{ki}\boldsymbol{v}_1}{\sqrt{\left(\boldsymbol{u}_1^H W_{ki}^H S_{k1} W_{ki}\boldsymbol{u}_1\right)\left(\boldsymbol{u}_1^H W_{ki}^H S_{k2} W_{ki}\boldsymbol{u}_1\right)}}\right|.$$

For the purpose of symmetry between numerator and denominator, we have replaced LS_{ki}^{source} in the numerator by its definition $W_{ki}^H LS_k W_{ki}$. The resulting formula is analogous to the calculation of lagged coherence at the sensor level (Eq. (1)). The source-reconstructed lagged coherence $\lambda^{source}(k, i)$ takes a value between 0 and 1, and can be calculated for every frequency, and every source location of interest.

Results

Lagged coherence measures phase consistency over time

Lagged coherence is a frequency-indexed measure that varies as a function of lag. The calculation of lagged coherence is described in detail in the Calculating lagged coherence section. To illustrate its dependence on frequency and lag, we zoomed in on a posterior MEG recording site during an eyes-closed resting-state recording. Fig. 3 displays lagged coherence as a function of lag at 10 Hz (Fig. 3A) and for a wide range of frequencies (Fig. 3B). Two observations stand out. First, lagged coherence decreases with increasing lag. This shows that the predictability of future phase decreases with time; in other words: phases that are further in the future are less predictable. Second, lagged coherence peaks in the frequency band where rhythmicity is expected, which is the alpha band at this posterior recording site during an eyes-closed measurement (Fig. 3B). At the same site, we also noted the presence of lagged coherence in the beta band, but this was much weaker and shorter lived.

In the remainder of this paper, we compare the performances of lagged coherence and power. We focus on the topographic map of these two measures, which we investigate in two frequency bands: alpha (7–15 Hz) and beta (20–28 Hz). In all analyses, the window length and the lag are equal to three cycles of that frequency. That is, both window length and lag are frequency-*dependent* when measured in seconds, but they are frequency-*independent* when measured in the number of cycles of the frequency for which lagged coherence is calculated. Here and in the following, we will speak about frequency *bands* rather than individual frequencies. This is because (1) power was calculated using a spectral smoothing of 4 Hz on both sides of the centre frequency, and (2) the calculation of lagged coherence involves an inherent restriction on its frequency resolution, induced by the three-cycle window length (see 2.5 and 2.6). The spectral smoothing for the power estimates (+/- 4 Hz) was chosen to approximate this restricted frequency resolution of lagged coherence. In all topographic plots in which power and lagged coherence are compared, this is done for the peak frequencies of the corresponding measure (as determined from their spectra). These peak frequencies may differ slightly, but the measures' frequency resolutions are comparable.

Lagged coherence is superior to power as a means to localise the sensorimotor rhythms in the brain, both in sensor and in source space

Here, we compare lagged coherence and power as measures for the identification and separation of rhythmic sources in ongoing MEG data. We evaluate these measures first at the sensor level, and then at the source level.

In Fig. 4A we show the average (over subjects) sensor level topographic maps of alpha and beta power (left) and lagged coherence (right) for synthetic planar gradiometer data collected during rest (733 ± 90 trials per subject). Because we depict the planar gradient,

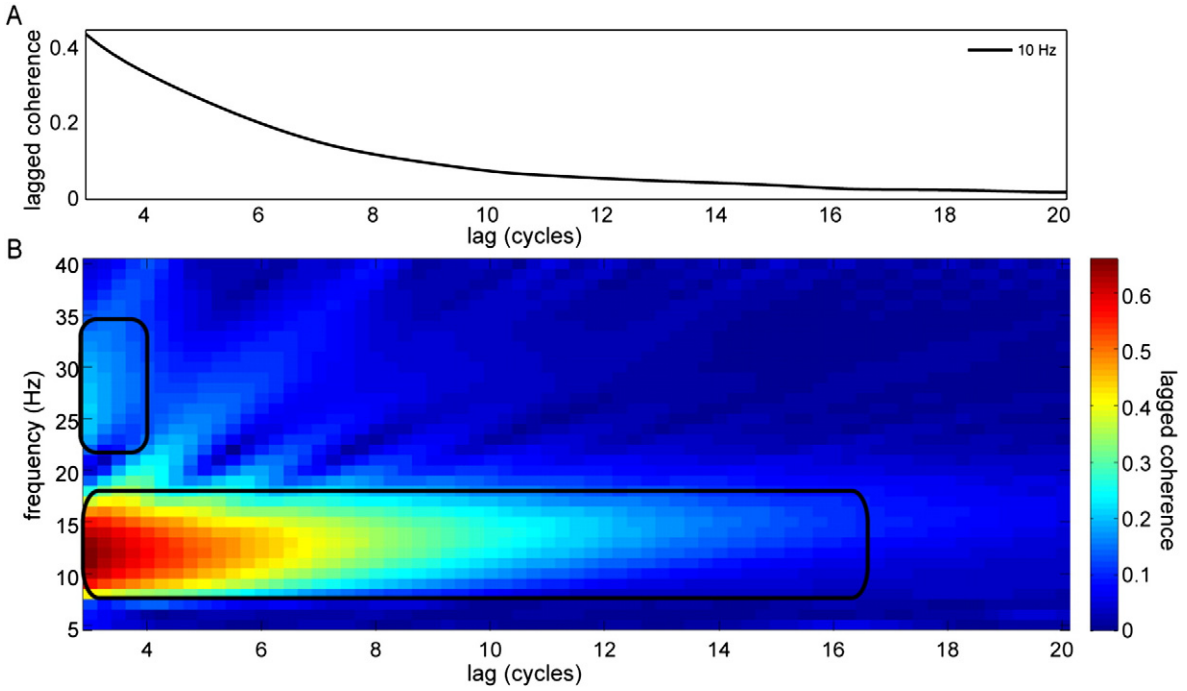

Fig. 3. Lagged coherence as a function of frequency and lag evaluates the typical duration of rhythms. (A) Lagged coherence can be used to evaluate the typical time period over which the phase remains consistent, namely by expressing it as a function of the lag between the epochs that are used for estimating between-epoch phase consistency. Here, we use a signal from a posterior MEG recording site, vary the lag from 3 to 20 cycles, and calculate lagged coherence at 10 Hz. It can be seen that lagged coherence monotonically decreases with lag. (B) By plotting lagged coherence as a function of both lag and frequency, the different rhythms can be compared with respect to the time period over which the phase remains consistent. It can be seen that the alpha band lagged coherence peak (between 10 and 15 Hz) remains high for much longer than the beta band lagged coherence peak (between 24 and 30 Hz), indicating that in this example data the posterior alpha phase remains consistent over a much longer time period than the posterior beta phase.

the topographies are focal and maximal directly above the source; see the Calculating planar gradient lagged coherence section. In the topographic maps of lagged coherence, at least for beta, clear peaks can be seen in left and right clusters of central recording sites, putatively above the left and right sensorimotor areas (Fig. 4A, right column). At the same sensorimotor locations, there are also local activity peaks in the topographic map of beta power, albeit less pronounced (Fig. 4A, left column). As we will show below, when moving to the source level the improved localisation on the basis of lagged coherence becomes evident for both alpha and beta oscillations.

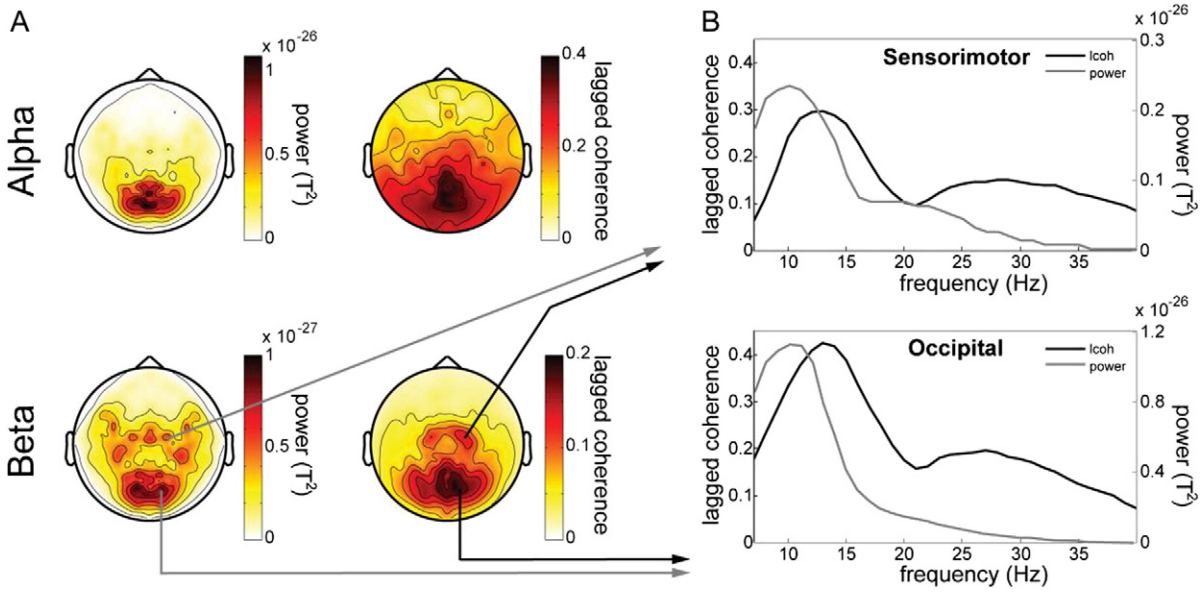

Fig. 4. Scalp topographies of beta band lagged coherence, but not power, allow for the identification of the sensorimotor rhythm. (A) Beta band (20–28 Hz) lagged coherence but not power allows for the identification of the putative sensorimotor sources from their scalp topographies. Power and lagged coherence were calculated for synthetic planar gradients, which have their maximum above the neuronal sources. Notice that the alpha band (7–15 Hz) lagged coherence topography is dominated by the spread of the high amplitude posterior source. The arrows indicate the spatial origin of the spectra shown in B. (B) Power (grey lines) is dominated by low frequencies to a much larger degree than lagged coherence (black lines). The lagged coherence spectra from both the putative sensorimotor (top) and posterior recording sites (bottom) are plotted on the same scales. Note that the peak frequencies of rhythmicity (13 and 28 Hz) are higher than those of power (10 and 20 Hz).

For one central and one posterior recording site, we also show power and lagged coherence spectra (Fig. 4B); spectra with almost identical shapes were obtained for other recording sites in these regions. The beta activity above the putative visual cortex can be identified more readily in the lagged coherence spectrum than in the power spectrum (Fig. 4B, lower window). The same holds to a lesser extent for the putative sensorimotor cortex (Fig. 4B, upper window): the lagged coherence spectrum has a separate peak in the beta range, whereas the power spectrum has no such peak. Instead, in the power spectrum, the alpha peak has a slight shoulder in the beta range. This shoulder is a bit more pronounced when power is calculated with a high spectral resolution (Fig. S1), but also then the power spectrum does not contain a distinct beta peak, such as is seen in the lagged coherence spectrum. Notice that the peak frequencies in the lagged coherence spectra are shifted to the right relative to the peak frequencies in the power spectra; we return to this in the discussion.

We also reconstructed lagged coherence at the source level, and compared this to source-reconstructed power. A commonly used method for source reconstruction of neuronal activity makes use of a form of adaptive spatial filtering, called beamforming (Van Veen et al., 1997; Gross et al., 2001; Liljestrom et al., 2005). We adapted the calculation of source-reconstructed power to the calculation of source-reconstructed lagged coherence, the details of which are described in the Source reconstruction of lagged coherence section.

Prior to comparing source-reconstructed lagged coherence with source-reconstructed power, we must briefly discuss an important shortcoming of source-reconstructed power when used to localise sources in a single experimental condition (i.e., without the use of an experimental contrast): depth bias (Sekihara and Scholz, 1996; Van Veen et al., 1997). Depth bias depends on the fact that leadfields for deep sources are much smaller than those for superficial sources. As a consequence, source-reconstructed power for these deep sources is affected much more by sensor level noise than superficial sources. This results in a 3D topographic map with a power peak at the centre of the head, and a gradual decrease towards the surface.

Several approaches have been taken to deal with this problem, the most common of which is to only consider topographic maps of power contrasts between two behavioural conditions. Here, we will only consider approaches that involve the source reconstruction of data within a single condition: leadfield normalisation and the neuronal activity index. The first method has been described in detail in Sekihara and Scholz (1996). In short, the leadfields are normalised to counteract their differential sensitivity to noise, thus compensating for the centre of head bias. The second method normalises the power by dividing the source-reconstructed power by an estimate of the noise power, resulting in the so-called neuronal activity index (NAI;(Van Veen et al., 1997). Interestingly, lagged coherence may provide another way of dealing with depth-bias when reconstructing oscillatory sources without a contrast, namely by circumventing depth-bias because it is a normalised measure, i.e. it does not deal with power.

In Fig. 5, we show a slice-based visualisation of the average (over subjects) 3D topographic maps of alpha band lagged coherence (top), leadfield normalised power (middle), and NAI (bottom). The source-reconstructed lagged coherence shows clear local alpha sources in both the occipital and the sensorimotor cortices (Fig. 5, top; remember that, at the sensor level, occipital and sensorimotor alpha band rhythms could not be separated). In contrast, the topographic maps of source-reconstructed power did not show local alpha sources in the sensorimotor cortex. Thus, neither leadfield normalisation (middle) nor the calculation of the NAI (bottom) was sufficient to identify these alpha sources. The source-reconstructed alpha topographic maps of lagged coherence, leadfield normalised power and NAI, were matched very closely by the source-reconstructed beta topographic maps (Fig. S2), and the superior performance of lagged coherence could thus be demonstrated for both alpha and beta oscillations.

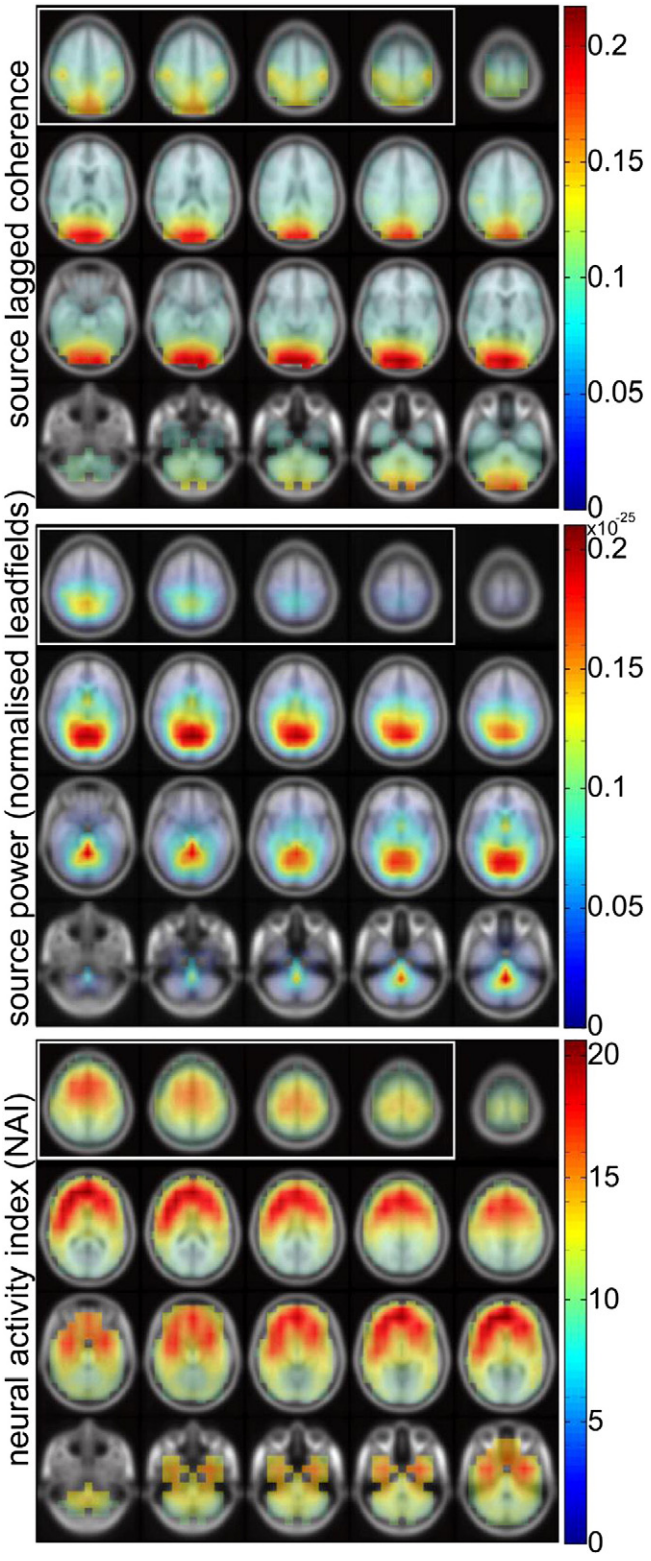

Fig. 5. Source-reconstructed topographies of lagged coherence but not power allow for the identification of the bilateral sensorimotor rhythm and localises the posterior alpha rhythm in the occipital cortex. Alpha sources in the posterior and the sensorimotor cortex can be identified from the source-reconstructed lagged coherence (top). These sources could not be localised using source-reconstructed power, despite the use of leadfield normalisation (middle), or normalisation by noise (bottom) to improve localisation.

The slice-based visualisations in Fig. 5 (alpha) and Fig. S2 (beta) strongly suggest that alpha and the beta band sensorimotor rhythms are fully separated from the occipital rhythms. To investigate this

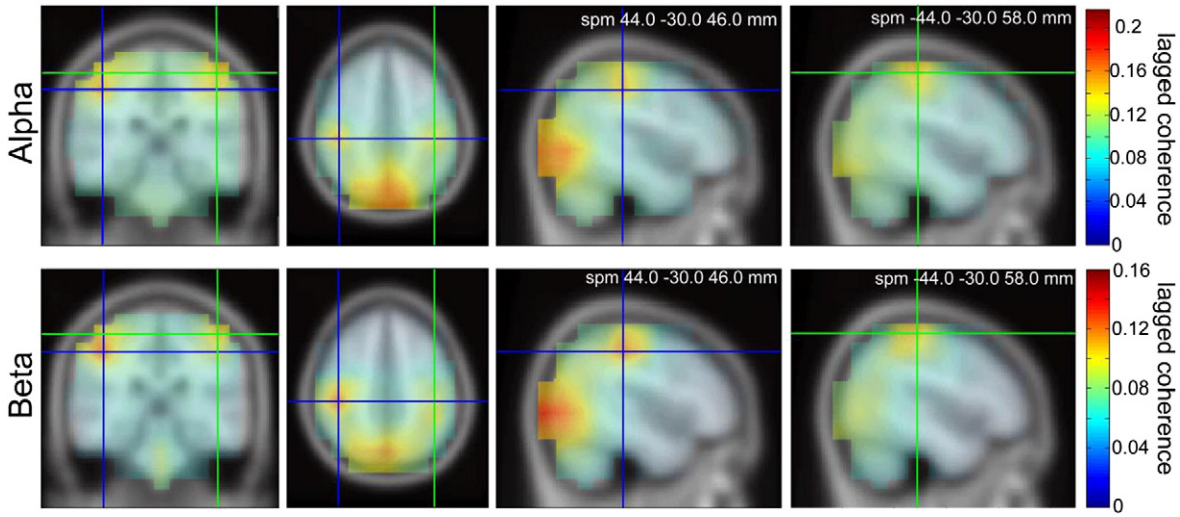

Fig. 6. Source-reconstructed lagged coherence topographies localise the sensorimotor alpha and beta oscillations to the same region and dissociate them from occipital sources. Brain slices through the right (blue) and the left (green) sensorimotor cortex show that the source-reconstructed lagged coherence is able to dissociate occipital from sensorimotor sustained activity. Source-reconstructed lagged coherence topographies show the left and right sensorimotor alpha (upper row) and beta (bottom row) rhythms, separated from the occipital sources. Note that the slices in the 1st column are viewed from the front and in the 2nd column from below, such that the right and left side of the subject are displayed on the left and right side of each image, respectively. As both horizontal cross-sections look nearly identical, we only show the horizontal cross-section with the lower of the two sensorimotor sources.

separability in more detail, we used cross sections through the local maxima of the sensorimotor rhythms in the 3D lagged coherence topographic maps. In Fig. 6, we show these cross sections in the sagittal, coronal and transverse directions. Again, both left and right sensorimotor sources are clearly dissociated from the occipital source as well as from each other.

Lagged coherence is superior to power in identifying top-down attentional modulations of the sensorimotor rhythms

Having identified the sensorimotor rhythms, we now study the way these rhythms are modulated by preparatory spatial attention. It has been well established that anticipation of a tactile stimulus on one hand decreases alpha and beta band power over the contralateral sensorimotor cortex (van Ede et al., 2010, 2011). Here, we replicate these results and show that there is also a decrease in the contralateral rhythmicity. More importantly, we show that using lagged coherence (but not power) this contralateral decrease can also be visualised without the use of an experimental contrast.

Previous work has shown that the sensorimotor cortex can be identified in source-reconstructed power by contrasting trials in which attention is oriented towards one versus the other hand (van Ede et al., 2011), trials in which attention is oriented to a particular hand versus trials in which attention is not oriented (van Ede et al., 2012), and trials resulting in fast versus slow responses to a tactile stimulus (van Ede et al., 2011). The contrast applied by van Ede et al. (2012) was applied to the same dataset as the one used in this paper. For clarity, we repeated this power contrast by comparing trials in which spatial attention was directed to the right or left hand, with trials in which no attentional cue was provided. For comparison, we also applied these attentional contrasts to lagged coherence and this showed that the attentional suppression of alpha and beta oscillations across the contralateral sensorimotor areas is also present for lagged coherence. The results for both contrasts are depicted in Figs. S3 and S4.

To date, the identification of task-related modulations of neuronal oscillations has always required the use of an experimental contrast (such as the attentional modulations described above). Given the superiority of lagged coherence in identifying the sources of neuronal oscillations without any contrast (Fig. 5), we asked if the attentional modulations in these oscillations could also be visualised without a contrast. For this, we separated trials in which the left hand was attended from trials in which the right hand was attended. Fig. 7 shows these sensor level topographic maps for alpha and beta oscillations, based on lagged coherence (Fig. 7A) and power (Fig. 7B). Especially for beta oscillations, the lagged coherence topographies for attending to the left or right hand each show a clear asymmetry: the local sensorimotor rhythm that is clearly visible ipsilateral to the attended hand, is virtually undetectable contralateral to the attended hand (Fig. 7A). This clear drop of the contralateral sensorimotor beta rhythm is not picked up to the same extent by the power topographies (Fig. 7B).

In Fig. 8, we show the corresponding source-reconstructed data. In both the alpha and beta band, a local sensorimotor source can be observed only ipsilateral to the attended side, but not contralateral. When attention is directed to the right hand, the sensorimotor sources in the left hemisphere are virtually undetectable (Fig. 8A, 4th column), whereas the ipsilateral sensorimotor sources remain clearly visible (Fig. 8B, 3rd column). Vice versa, when attending to the left hand, the sensorimotor sources in the left hemisphere remain clearly visible (Fig. 8B, 4th column), whereas the sources in the left hemisphere are virtually undetectable (Fig. 8A, 3rd column). Thus, when attention is directed to one of the hands, the sensorimotor alpha and beta sources in the contralateral hemisphere become virtually undetectable, whereas those in the ipsilateral hemisphere remain clearly visible. Again, for power no such patterns emerge (Fig. S5) unless a contrast is applied (Figs. S3 andS4).

Discussion

In this work, we started from a definition of rhythmicity as the consistency of the phase relations between time points that are separated by a fixed lag, and proposed a novel measure for it (lagged coherence). By construction, we expected lagged coherence to be better suited for identifying rhythmic neuronal activity than Fourier power, because the latter depends not only on waveform rhythmicity, but also on waveform amplitude. We demonstrated this empirically for MEG data at both the sensor- and at the source level.

This demonstration is discussed in the following section. Next, we discuss the dependence of lagged coherence on amplitude, lag and window length, and we address the observed differences in peak-frequency between the power and lagged coherence spectra. Finally, we discuss the reasons behind the superior performance of lagged coherence.

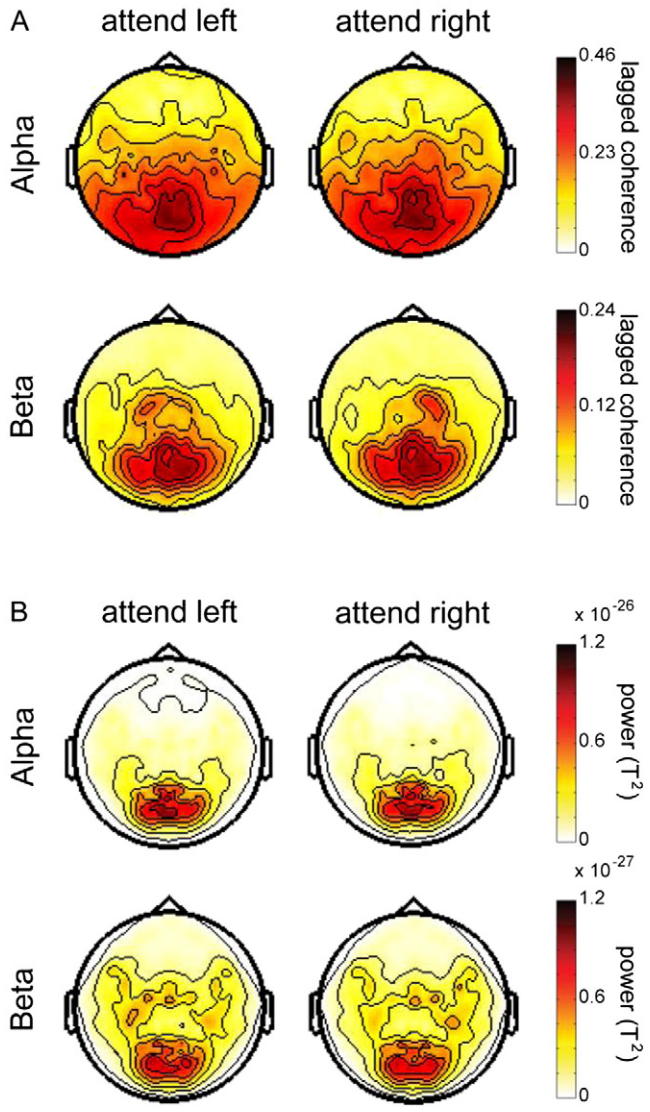

Fig. 7. Scalp topographies of beta band lagged coherence but not power show attentional modulation of the contralateral sensorimotor rhythm. Lagged coherence and power was calculated for the period 0.5–1.5 s after the offset of a spatial attention cue (left versus right thumb) indicating the side were a tactile stimulus would be presented. (A) When attending the left thumb, lagged coherence shows a clear sensorimotor beta peak over the left (ipsilateral), but not the right (contralateral) hemisphere. Vice versa, when attending the right thumb, the sensorimotor beta peak is only visible over the right hemisphere. No clear attentional modulations are visible in the alpha band. (B) Neither the alpha nor the beta band power topographies show a clear focal attentional modulation.

Rhythmicity as the key identifier of neuronal oscillations

This is the first work that draws attention to the importance of rhythmicity as compared to Fourier power for the identification of neuronal oscillations and their task-related modulations. Obviously, the concept of rhythmicity is present in more theoretical papers that advocate the role of oscillations in neuronal communication (Fries, 2005; Tiesinga et al., 2008): rhythmicity combined with between-site coherence provides a condition in which a receiving population at one site can predict the input from a sending population at another site, allowing for a phase adjustment that makes this input more or less effective. The present paper uses rhythmicity for a more practical objective, namely the identification of neuronal oscillations. In short, we showed that rhythmicity (as quantified by lagged coherence) outperforms Fourier power as a means to identify and localise neuronal oscillations, and allows for a more straightforward way to study their task-related modulations.

To be more precise, we showed that, unlike power, lagged coherence of ongoing data localises multiple concurrent neuronal oscillations to the appropriate neocortical areas: the sensorimotor alpha and beta rhythms could be identified and separated from the visual activity within each experimental condition. Even when this spatial identification did not allow for a clear separation at the sensor level (as was the case for alpha, but not for beta oscillations), the measure could be combined with existing source reconstruction techniques to improve the spatial specificity and separate the visual from the sensorimotor alpha and beta rhythms within a single experimental condition. In contrast, in our previous work – using Fourier power – occipital and sensorimotor alpha and beta rhythms could never be separated based on the topographic map. A contrast between conditions, in which the sensorimotor sources were differentially active, was always required to visualise them (van Ede et al., 2011, 2012, 2014). This is in agreement with common practice in studies on the sensorimotor rhythms (Cheyne, 2013).

We should note that Liljestrom et al. (2005) were able to source reconstruct Fourier power such that they could identify the sensorimotor alpha and beta sources in single subject analyses. They did this in a post-processing step in which they consecutively removed the field produced by the strongest source: after identifying this source, its field was included in the noise term (i.e. in the denominator) during the normalisation step that transforms raw source-reconstructed power into the neural activity index (NAI). This post-processing made it possible to visualise the fields from the sensorimotor alpha and beta sources. Our results are in agreement with their findings that sensorimotor alpha and beta sources exist in ongoing data and roughly co-localise with one another. At the same time, we could expand on their results such that, using lagged coherence, sensorimotor sources could also be identified after averaging over subjects. Furthermore, using lagged coherence, the sensorimotor alpha sources could be visualised together with the occipital alpha sources; i.e. there was no need for post-processing to remove the occipital sources. Although the co-localisation of the alpha and beta sources in this study may spur speculation on the harmonic nature of the sensorimotor beta, we cannot in good conscience claim that the co-localisation in our study provides strong evidence for the harmonic nature of the sensorimotor beta, because neither the spatial nor spectral resolutions suffice for such a claim. In fact, against such an account, we have recently demonstrated that the sensorimotor beta oscillations cannot be a harmonic of the sensorimotor alpha rhythm because they have a different connectivity profile (van Ede and Maris, 2013). Furthermore, using lagged coherence, no alpha sources were found in parietal cortex. Other studies that compared source-reconstructed alpha power between experimental conditions did find alpha sources in parietal cortex (Jokisch and Jensen, 2007; Tuladhar et al., 2007; Van Dijk et al., 2008; Van der Werf et al., 2010).

We showed not only that lagged coherence was better able to identify the sensorimotor rhythms, it was also better able to identify their task-related modulation – here studied for preparatory spatial attention to the left or right hand. We show that, within each attention condition, there were no detectable local sensorimotor alpha or beta sources of rhythmic activity contralateral to the attended side. In those same conditions the ipsilateral sensorimotor alpha and beta sources were clearly visible. The extent to which the contralateral alpha and beta rhythms disappear had not been shown before, as it was not previously possible to identify and visualise the sensorimotor rhythms within each condition separately. However, these results are in accordance with the well-established decrease in contralateral sensorimotor alpha and beta power during spatial attention (van Ede et al., 2011; Bauer et al., 2012; Cheyne, 2013). The new ability to identify oscillatory sources within a single experimental condition provides new opportunities to study these oscillations and their modulations by task-demands in a more straightforward way.

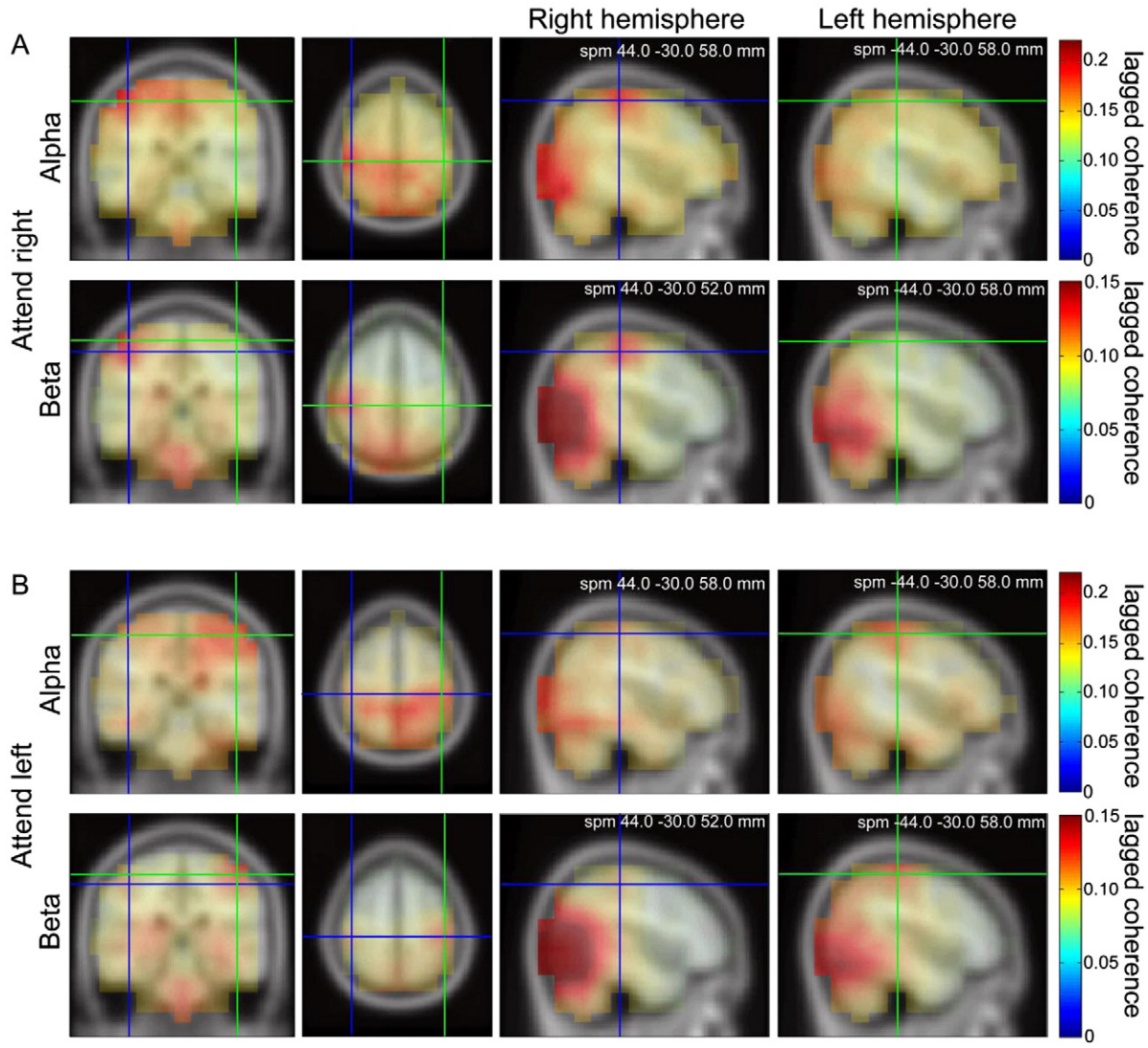

Fig. 8. Source-reconstructed lagged coherence topographies which are obtained from different attentional conditions (right versus left thumb) show lateralised rhythmicity in both the alpha and the beta bands. Lagged coherence and power was calculated for the period 0.5–1.5 s after the offset of a spatial attention cue (left versus right thumb) indicating the side were a tactile stimulus would be presented. (A) When attending to the right thumb, sensorimotor sources in the left (contralateral) hemisphere virtually disappear for both the alpha (upper row) and beta bands (lower row). (B) Vice versa, when attending the left thumb, sensorimotor sources in the right (contralateral) hemisphere virtually disappear for both the alpha (upper row) and beta bands (lower row). Note that the slices in the first column are viewed from the front and those in the second column from below. Thus, the intersection of the blue lines indicates the location of the sensorimotor source in the right hemisphere, whereas the intersection of green lines indicates the sensorimotor source in the left hemisphere.

Using lagged coherence, the ability to identify rhythms within a single experimental condition allows one to distinguish between rhythms that are modulated by the experimental variable and those that are not. In fact, the rhythms that are not modulated by the experimental variable can only be identified in the separate experimental conditions, whereas the rhythms that *are* modulated can also be identified in the difference between the experimental conditions. Using power, it is more difficult to distinguish between rhythms which are and which are not modulated by an experimental variable, because it is more difficult to identify the rhythms within the separate experimental conditions.

Amplitude-dependence of lagged coherence

In this paper, we have pointed out more than once that lagged coherence is an amplitude-independent measure of rhythmicity. Although this is true in cases where the signal is noise-free, we have not discussed cases in which the signal also contains noise. When the amplitude of the rhythmic signal and the amplitude of the noise are fully correlated, lagged coherence is indeed unaffected. In contrast, when the amplitude of either the rhythm or the noise term changes (effectively changing the signal-to-noise ratio; SNR), this does affect lagged coherence. In fact, the value of lagged coherence can be interpreted as the proportion of the activity that is due to a perfectly predictable rhythm. In other words, lagged coherence in a given frequency band can be considered as the ratio of the amplitude of a perfectly rhythmic signal component to the amplitude of the whole signal (including arrhythmic components) in that same band. Thus, noise, which is generally arrhythmic, causes a reduction of lagged coherence, because the noise increases the magnitude of the denominator in the calculation of lagged coherence (see the Calculating lagged coherence section). In contrast, the special case of rhythmic noise (such as 50 or 60 Hz line noise) will increase lagged coherence at that frequency.

The parameters of lagged coherence

Lagged coherence depends on two parameters: the length of the windows for which the Fourier coefficients are calculated, and the lag between these windows. The first parameter, window length, determines the frequency resolution of the Fourier coefficients. Therefore,

in applications that require a high frequency resolution, a long window is required. However, window length also affects the minimal lag required to ensure that the epochs do not overlap. The longer the epochs, the more the Fourier coefficients are determined by parts of the signal that are very separated in time. Because the brain does not produce perfect rhythms (i.e. oscillatory activity with a perpetually linear phase) lagged coherence decreases with increasing window length.

Lagged coherence also decreases with the second parameter, the lag between the windows as we have demonstrated in Fig. 3. Again, this is because the brain does not produce oscillatory activity with a perpetually linear phase. Interestingly, although beyond the scope of this paper, new insights into neuronal oscillations can be gained by investigating the influence of lag. For example, when using very long lags (>20 cycles), we noticed periodic variations in lagged coherence, suggestive of phase-phase coupling between ultra-slow frequencies (±0.5 Hz) and alpha activity. We also observed phase-phase coupling between alpha and beta activity as seen in Fig. 3B. There, the lagged coherence of 20 Hz (beta) oscillations peaks after approximately 4, 6 and 8 beta cycles. This may suggest that the phase of the 20 Hz activity is reset during a particular phase of the 10 Hz activity. Alternatively, these peaks may reflect the non-sinusoidal waveform of the alpha rhythm: if the 10 Hz waveform has sharp troughs or peaks, these might dominate the estimate of the 20 Hz Fourier coefficients once every 0.1 s (i.e. every two cycles at 20 Hz). Note that we do not claim that, in general, neuronal activity in the beta band is the first harmonic of a non-sinusoidal alpha band rhythm. This is because (1) we only investigated the dependence of lagged coherence on its parameters in one subject and in one posterior MEG recording site, and (2) we did not quantify how much of the beta band lagged coherence can be explained by this harmonic component. The example data discussed here merely suggests that lagged coherence as a function of both lag and frequency might be an interesting tool to investigate phase-phase coupling in future studies.

The observed difference between peak power and peak lagged coherence

As can be seen in Fig. 4B, there was a systematic difference between peak power and peak lagged coherence. In our analyses, alpha peaked at approximately 11 Hz for power, and at approximately 13 Hz for lagged coherence; beta did not 'peak' to the same extent, but the top of the bump was at approximately 20 Hz for power, and 27 Hz for lagged coherence. The difference between these peak frequencies may in part be due to the 1/*f* component in the power spectrum (Pritchard, 1992), which is absent in the lagged coherence spectrum. This 1/*f* component in the power spectrum may especially affect the beta peak frequency, as most of the beta power is due to the 1/*f* component.

In addition to the 1/*f* component, there may be other reasons for the observed frequency shift, as we explore below. We noticed that the peak frequency of alpha lagged coherence (but not power) changed when we increased the number of cycles used to estimate each Fourier coefficient (i.e. the window length). Namely, when we used only 1 cycle, the alpha peak was at 15 Hz, and when the number of cycles was increased to 6 cycles the alpha peak decreased to 11 Hz and then remained at 11 Hz when the number of cycles was further increased. This effect of window length on lagged coherence was independent of the lag at which this relation was quantified.

We can only speculate on the physiological reasons behind this frequency shift and it dependence on window length. This property of lagged coherence may result from the fact that, for each frequency, lagged coherence measures to what extent the signal's phase is predictable, not the extent to which the signal approximates a pure oscillation of that frequency. This allows for the possibility that waveforms which are non-sinusoidal may be most predictable at a particular phase of their rhythm. For example, supposing the ongoing sensorimotor alpha rhythm contains sharp troughs (as we observed in unpublished results; and which matches the profile of lagged coherence over lag in Fig. 3B). If these sharp troughs exist and are more predictable than other phases of the alpha rhythm, this may explain the observed frequency shift when Fourier coefficients depend on very few cycles. Concretely, let us analyse an 11 Hz alpha rhythm with sharp troughs using a window length of 1 cycle for each Fourier coefficient. Crucially, the waveform of the non-sinusoidal 11 Hz rhythm also has energy in higher frequencies and this energy will affect the phase of the Fourier coefficients. As a result, compared to lagged coherence at 11 Hz, the one at 15 Hz will be driven more by the sharp troughs. Now, if the timing of these troughs is more predictable than the timing of other segments of the 11 Hz rhythm, this would predict a lagged coherence peak at a frequency that is higher than 11 Hz (e.g. at 15 Hz). On the other hand, when we would analyse the same signal using a window length of 6 cycles, the relative timing of the troughs (namely once every .09 s, or at 11 Hz), will prevent the Fourier coefficients at 15 Hz to be dominated by these troughs. This is because each trough will occur at a different phase of the 15 Hz oscillation. Consequently, when using more cycles to estimate Fourier coefficients, the peak lagged coherence frequency will more reflect the main frequency of the rhythm rather than higher frequency components in the waveform.

Thus, we hypothesise that the alpha rhythm contains sharp troughs which are more predictable than other parts of the alpha rhythm. We would like to emphasise once more that this hypothesis is highly speculative and that other, as yet unidentified, phenomena may play a role as well.

Why lagged coherence may be better suited to identify rhythms than power

We speculate that neuronal oscillations, as measured in field potentials (i.e. the periodic synchronous fluctuations of EPSPs (see Jagadeesh et al., 1992, and Volgushev et al., 1998), may be better quantified by measuring rhythmicity rather than power. We speculate that the energy in a frequency band consists of both rhythmic activity and transients. The occurrence of transients with most of their energy in a particular frequency band) has been reported, and has been suggested to involve a different underlying mechanism than rhythmic activity in the same frequency band (Riehle et al., 1997; Fetz, 2013). Our measure of rhythmicity was insensitive to such transient activity and this may account for part of the improved identification of neuronal oscillations. In principle, distinguishing between rhythmic and transient activity is also possible using matching pursuit (Mallat and Zhang, 1993). However, unlike matching pursuit, which requires post-processing of the decomposition, lagged coherence provides a direct measure of rhythmicity.

It should be pointed out here that lagged coherence is not restricted to the detection of sinusoid rhythms. In fact, if a signal contains transient events that occur with regular inter-event intervals, these rhythmic events may also show up in the lagged coherence spectrum. Namely, as a result of the consistent time relation between the transient events, they may cause a consistent phase relation across non-overlapping epochs for certain frequencies. In addition, we should warn potential users that when low-, high- or band-pass filters are applied to the data, transients in the signal may introduce short-lived oscillations in the filtered signal. Interpretation problems related to this type of false oscillatory phenomena (false ripples) have been described previously by Benar et al. (2010).

Lagged coherence may improve the identification of neural oscillations not only by its ability to separate rhythmic from arrhythmic activity, but also by its ability to spatially separate multiple rhythmic sources that differ vastly in amplitude. This is because, unlike power, lagged coherence is a normalised measure that is unaffected by amplitude (with some differences due to SNR, see 4.2). For example, if the posterior oscillations are much larger in amplitude than those in the sensorimotor cortices, then this will explain their dominance in measures of power. However, if, despite their difference in amplitude, the posterior and sensorimotor oscillations are equally rhythmic, they will have highly comparable lagged coherence (with some differences due

to SNR, see the Amplitude-dependence of lagged coherence section). Thus, using lagged coherence, neuronal oscillations can be identified on the basis of their rhythmicity alone, without being occluded by strong (rhythmic or arrhythmic) sources such as the posterior alpha rhythm.

Appendix A. Supplementarty data

Supplementary data to this article can be found online at http://dx.doi.org/10.1016/j.neuroimage.2015.06.003.

References

Bastiaansen, M.C., Knosche, T.R., 2000. Tangential derivative mapping of axial MEG applied to event-related desynchronization research. Clin. Neurophysiol. 111, 1300–1305.

Bauer, M., Kennett, S., Driver, J., 2012. Attentional selection of location and modality in vision and touch modulates low-frequency activity in associated sensory cortices. J. Neurophysiol. 107, 2342–2351.

Benar, C.G., Chauviere, L., Bartolomei, F., Wendling, F., 2010. Pitfalls of high-pass filtering for detecting epileptic oscillations: a technical note on "false" ripples. Clin. Neurophysiol. 121, 301–310.

Bosman, C.A., Lansink, C.S., Pennartz, C.M.A., 2014. Functions of gamma-band synchronization in cognition: from single circuits to functional diversity across cortical and subcortical systems. Eur. J. Neurosci. 39, 1982–1999.

Bruns, A., 2004. Fourier-, Hilbert- and wavelet-based signal analysis: are they really different approaches? J. Neurosci. Methods 137, 321–332.

Buzsáki, G., Draguhn, A., 1926–1929. Neuronal oscillations in cortical networks. Science 304, 2004.

Chan, V., Starr, P.A., Turner, R.S., 2011. Bursts and oscillations as independent properties of neural activity in the parkinsonian globus pallidus internus. Neurobiol. Dis. 41, 2–10.

Cheyne, D.O., 2013. MEG studies of sensorimotor rhythms: a review. Exp. Neurol. 245, 27–39.

Davis, N.J., Tomlinson, S.P., Morgan, H.M., 2012. The role of beta-frequency neural oscillations in motor control. J. Neurosci. 32, 403–404.

Düzel, E., Penny, W.D., Burgess, N., 2010. Brain oscillations and memory. Curr. Opin. Neurobiol. 20, 143–149.

Engel, A.K., Fries, P., 2010. Beta-band oscillations — signalling the status quo? Curr. Opin. Neurobiol. 20, 156–165.

Fetz, Eberhard E., 2013. Volitional control of cortical oscillations and synchrony. Neuron 77, 216–218.

Freyer, F., Aquino, K., Robinson, P.A., Ritter, P., Breakspear, M., 2009. Bistability and non-Gaussian fluctuations in spontaneous cortical activity. J. Neurosci. 29, 8512–8524.

Fries, P., 2005. A mechanism for cognitive dynamics: neuronal communication through neuronal coherence. Trends Cogn. Sci. 9, 474–480.

Fries, P., 2009. Neuronal gamma-band synchronization as a fundamental process in cortical computation. Annual Review of Neuroscience vol. 32. Annual Reviews, Palo Alto, pp. 209–224.

Govindan, R., Raethjen, J., Arning, K., Kopper, F., Deuschl, G., 2006. Time delay and partial coherence analyses to identify cortical connectivities. Biol. Cybern. 94, 262–275.

Gross, J., 2014. Analytical methods and experimental approaches for electrophysiological studies of brain oscillations. J. Neurosci. Methods 228, 57–66.

Gross, J., Kujala, J., Hamalainen, M., Timmermann, L., Schnitzler, A., Salmelin, R., 2001. Dynamic imaging of coherent sources: studying neural interactions in the human brain. Proc. Natl. Acad. Sci. 98, 694–699.

Jagadeesh, B., Gray, C., Ferster, D., 1992. Visually evoked oscillations of membrane potential in cells of cat visual cortex. Science 257, 552–554.

Jokisch, D., Jensen, O., 2007. Modulation of gamma and alpha activity during a working memory task engaging the dorsal or ventral stream. J. Neurosci. 27, 3244–3251.

Kaneoke, Y., Vitek, J.L., 1996. Burst and oscillation as disparate neuronal properties. J. Neurosci. Methods 68, 211–223.

Koepsell, K., Wang, X., Hirsch, J.A., Sommer, F.T., 2010. Exploring the function of neural oscillations in early sensory systems. Front. Neurosci. 4, 53.

Lachaux, J.P., Rodriguez, E., Martinerie, J., Varela, F.J., 1999. Measuring phase synchrony in brain signals. Hum. Brain Mapp. 8, 194–208.

Liljestrom, M., Kujala, J., Jensen, O., Salmelin, R., 2005. Neuromagnetic localization of rhythmic activity in the human brain: a comparison of three methods. NeuroImage 25, 734–745.

Mallat, S.G., Zhang, Z.F., 1993. Matching pursuits with time-frequency dictionaries. IEEE Trans. Signal Process. 41, 3397–3415.

Muthuraman, M., Govindan, R., Deuschl, G., Heute, U., Raethjen, J., 2008. Differentiating phase shift and delay in narrow band coherent signals. Clin. Neurophysiol. 119, 1062–1070.

Oostenveld, R., Fries, P., Maris, E., Schoffelen, J.M., 2011. FieldTrip: open source software for advanced analysis of MEG, EEG, and invasive electrophysiological data. Comput. Intell. Neurosci. 2011, 156869.

Percival, D.B., Walden, A.T., 1993. Spectral Analysis For Physical Applications: Multitaper And Conventional Univariate Techniques. Cambridge Univ. Press, Cambridge, UK.

Pritchard, W.S., 1992. The brain in fractal time — 1/f-like power spectrum scaling of the human electroencephalogram. Int. J. Neurosci. 66, 119–129.

Riehle, A., Grun, S., Diesmann, M., Aertsen, A., 1997. Spike synchronization and rate modulation differentially involved in motor cortical function. Science 278, 1950–1953.

Rosenberg, J.R., Amjad, A.M., Breeze, P., Brillinger, D.R., Halliday, D.M., 1989. The Fourier approach to the identification of functional coupling between neuronal spike trains. Prog. Biophys. Mol. Biol. 53, 1–31.

Sekihara, K., Scholz, B., 1996. Generalized Wiener estimation of three-dimensional current distribution from biomagnetic measurements. IEEE Trans. Biomed. Eng. 43, 281–291.

Tiesinga, P., Fellous, J.M., Sejnowski, T.J., 2008. Regulation of spike timing in visual cortical circuits. Nat. Rev. Neurosci. 9, 97–109.

Tuladhar, A.M., ter Huurne, N., Schoffelen, J.-M., Maris, E., Oostenveld, R., Jensen, O., 2007. Parieto-occipital sources account for the increase in alpha activity with working memory load. Hum. Brain Mapp. 28, 785–792.

Van der Werf, J., Jensen, O., Fries, P., Medendorp, W.P., 2010. Neuronal Synchronization in Human Posterior Parietal Cortex during Reach Planning. J. Neurosci. 30, 1402–1412.

Van Dijk, H., Schoffelen, J.-M., Oostenveld, R., Jensen, O., 2008. Prestimulus oscillatory activity in the alpha band predicts visual discrimination ability. J. Neurosci. 28, 1816–1823.

van Ede, F., Maris, E., 2013. Somatosensory demands modulate muscular beta oscillations, independent of motor demands. J. Neurosci. 33, 10849–10857.

van Ede, F., Jensen, O., Maris, E., 2010. Tactile expectation modulates pre-stimulus beta-band oscillations in human sensorimotor cortex. NeuroImage 51, 867–876.

van Ede, F., de Lange, F., Jensen, O., Maris, E., 2011. Orienting attention to an upcoming tactile event involves a spatially and temporally specific modulation of sensorimotor alpha- and beta-band oscillations. J. Neurosci. 31, 2016–2024.

van Ede, F., Köster, M., Maris, E., 2012. Beyond establishing involvement: quantifying the contribution of anticipatory α- and β-band suppression to perceptual improvement with attention. J. Neurophysiol. 108, 2352–2362.

van Ede, F., de Lange, F.P., Maris, E., 2014. Anticipation increases tactile stimulus processing in the ipsilateral primary somatosensory cortex. Cereb. Cortex 24, 2562–2571.

Van Veen, B.D., van Drongelen, W., Yuchtman, M., Suzuki, A., 1997. Localization of brain electrical activity via linearly constrained minimum variance spatial filtering. IEEE Trans. Biomed. Eng. 44, 867–880.

Volgushev, M., Chistiakova, M., Singer, W., 1998. Modification of discharge patterns of neocortical neurons by induced oscillations of the membrane potential. Neuroscience 83, 15–25.

Wacker, M., Witte, H., 2013. Time-frequency techniques in biomedical signal analysis. a tutorial review of similarities and differences. Methods Inf. Med. 52, 279–296.

Ward, L.M., 2003. Synchronous neural oscillations and cognitive processes. Trends Cogn. Sci. 7, 553–559.